



ROLE OF IQGAP2 DEPENDING ON THE RAS SUBCELLULAR LOCALIZATION: IMPLICATIONS ON THYROID CANCER

MASTER IN MOLECULAR BIOLOGY AND BIOMEDICINE
UNIVERSITY OF CANTABRIA
2017/2018

EVA MONTE SERRANO

DIRECTORS: PIERO CRESPO, BERTA CASAR

Cellular and Molecular Signaling Department (IBBTEC)

ABSTRACT

Thyroid cancer is the most common endocrine malignancy worldwide. In 70% of the cases, it is related to mutation that activate the Ras-Raf-MEK-ERK cascade, a well-known pathway related with cellular transformation, proliferation and tumour progression. The high frequency of aberrant Ras expression in this pathway results in the more aggressive and worse prognosis thyroid carcinomas. Moreover, Ras proteins are distributed in different types of plasma membrane and endomembrane microdomains: endoplasmic reticulum, lipid rafts, disorder membrane and the Golgi complex. It has been shown that compartmentalization dictates the use of Ras effectors, the intensity of their signals and consequently the biological response of the cells. Furthermore, the last studies shown the participation of scaffold proteins in the spreading of site-specific Ras signals to enhance the activation of ERK targets. However, although IQGAP2 expression is downregulated in some neoplasms, their role in thyroid cancer is not well documented yet. We have generated by CRISPR/CAS9 genome editing an IQGAP2 knock out stable PCCL3 cells lines expressing H-RasV12 in the different subcellular localizations, with the purpose of study their proliferative, migrative and invasive behavior. Moreover, we have used the chick chorioallantoic membrane embryo model to determine the role of IQGAP2 in thyroid tumor progression *in vivo*. This information can contribute to determine the participation of IQGAP2 in thyroid cancer and develop new cancer therapies where therapeutic agents are used to suppress the oncogenic signaling through the Ras-ERK axis, hopefully improving tumor control and survival of thyroid cancer patients in the future.

LIST OF CONTENTS

1.	Background and current state of the topic.....	2
1.1	Thyroid cancer	2
1.2	The Ras-ERK pathway.....	4
1.2.1	Sublocalizations of Ras	6
1.2.2	Scaffolds of the Ras-ERK pathway	8
1.3	Progress in Piero Crespo's lab	10
2	Objectives.....	14
3	Materials y methods.....	15
4	Results	22
5	Discussion.....	29
6	Conclusion	31
7	Future perspectives.....	32
8	References	33

1. BACKGROUND AND CURRENT STATE OF THE TOPIC

1.1 THYROID CANCER

The thyroid is a highly vascular, brownish-red gland located anteriorly in the lower neck, extending from the level of the fifth cervical vertebra down to the first thoracic. Histologically, a normal thyroid gland is compound of two main parenchymal cell types: follicular cells and parafollicular cells (Figure 1). A dysregulation of the proliferation of these cells could lead to thyroid cancer, that is the most common endocrine malignancy worldwide (Carling & Udelsman, 2014; Riesco-Eizaguirre & Santisteban, 2007). However, although deaths due to thyroid cancer are uncommon, in the last four decades its prevalence has increased steadily.

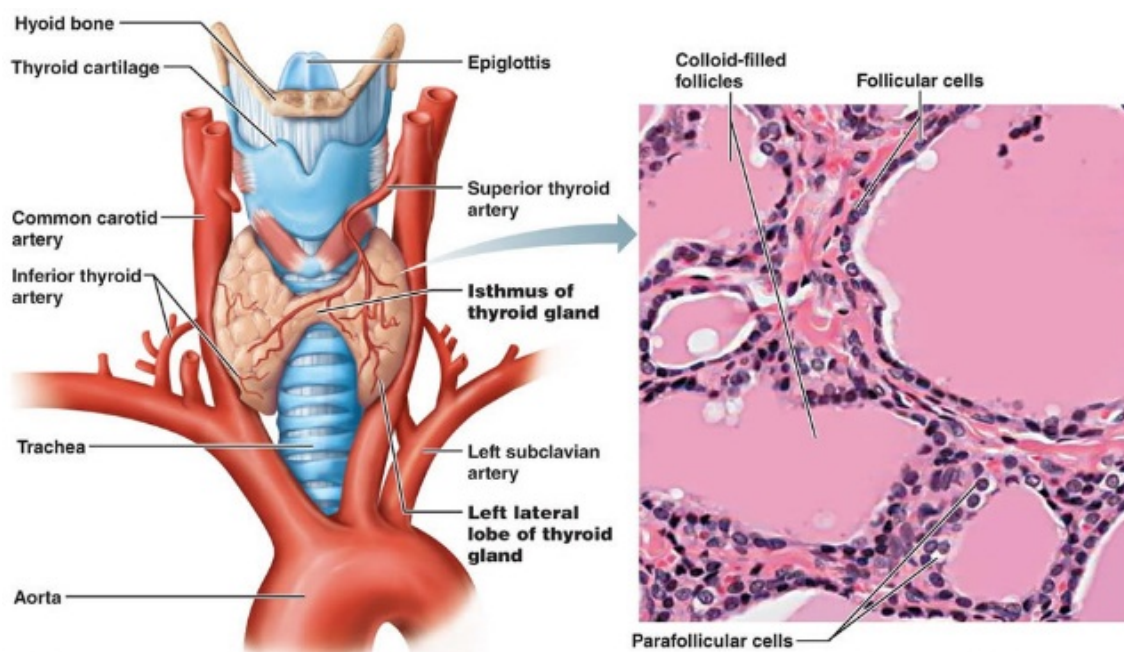


Figure 1 | (A) Anatomy of the normal thyroid gland. The thyroid has an inner true capsule that project extensions within the substance of the gland forming numerous septae, which divide it into lobes and lobules **(B) Photomicrograph of thyroid gland (145X).** The lobules are composed of follicles, the structural units of the gland, which consist of a layer of simple epithelium enclosing a colloid-filled cavity. This colloid (pink on hematoxylin and eosin stain) contains an iodinated glycoprotein, iodothyroglobulin, a precursor of thyroid hormones. Follicles vary in size, depending upon the degree of distention, and they are surrounded by dense plexuses of fenestrated capillaries, lymphatic vessels, and sympathetic nerves. Figure from Pearson Education, Inc (2015).

It is well known that thyroid carcinomas can arise from the follicular cells appearing well-differentiated thyroid carcinoma (WDTC), which include two main subtypes: papillary thyroid carcinoma (PTC) and follicular thyroid carcinoma (FTC); intermediate/poorly differentiated thyroid carcinoma (PDTC) and anaplastic thyroid carcinoma (ATC) (Figure 2). Most of the time, 93%, thyroid cancers emerge from the follicular cells and are WDTC, especially PTC

which accounts for 80–85% of all thyroid carcinomas. Conversely, and fortunately although their very aggressive behavior and their worse prognosis, PDTC and ATC are uncommon, with a frequency of 6% and 1–2% (Carling & Udelsman, 2014; Zaballos & Santisteban, 2017). Moreover, these thyroid carcinomas metastasize at a relatively high frequency mainly toward lung, liver and bone (Carling & Udelsman, 2014; Riesco-Eizaguirre & Santisteban, 2007).

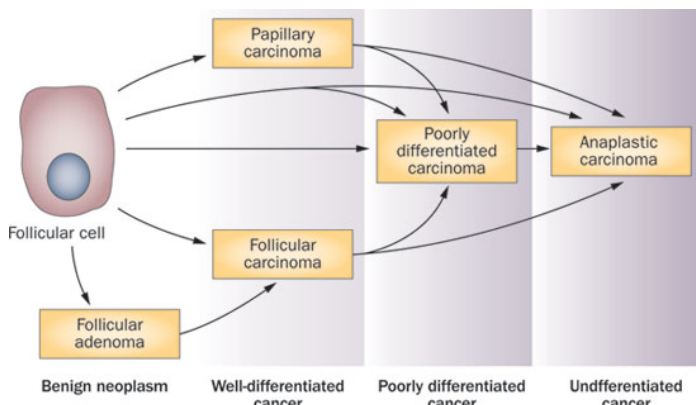


Figure 2 | Scheme of the different thyroid cancer originated from follicular cells. Carcinomas derived from thyroid follicular cells can be subdivided into four main different types based on histological architecture and cellular morphology. Thyroid carcinomas that retain differentiated properties are termed WDTC (include

PTC and FTC) PDTC and ATC. Figure from Nikiforov & Nikiforova (2011).

On the other hand, the parafofollicular cells give rise to medullary thyroid cancer, other case of uncommon thyroid malignance that compromise around 3% of thyroid carcinomas (Naoum, Morkos, Kim, & Arafat, 2018).

Thyroid cancer arising from follicular cells is wildly related to mutations that activate the mitogen-activated protein kinase (MAPK) cascades (70% of the cases) (Zaballos & Santisteban, 2017). The first component to be identified as an oncogene for thyroid cancer was Ras, a GTPase protein. Ras can present mutations that affect the GTP-binding domain or the GTPase domain, resulting in a continuous activation of the protein facilitating tumor development. The frequency with which mutant Ras contribute to thyroid cancer change between 7 to 62% depending of the type. Ras mutations are not very common in WDTC. Conversely, their frequency increase up 52-55% in PDTC and ATC, those more aggressive and with less survival rate, supporting a role for Ras in the progression to aggressive forms of thyroid carcinomas (Figure 3) (Riesco-Eizaguirre & Santisteban, 2007; Zaballos & Santisteban, 2017). For this, henceforth, in this project, we will focus in mutant Ras and the thyroid tumors originated from follicular cells.

However, it is known other possibility is that thyroid cancer is caused by oncogenic mutations of B-RAF, another component of the Ras-ERK pathway. These happens because mutant B-RAF destabilize its inactive structure, so that facilitates an active conformation and resulting in constitutive catalytic activation. Specifically, the V600E mutant of B-RAF is the most frequently genetic cause in PTC, present in about 29–83% of cases. However, this mutation type has not found in any form of FTC (Riesco-Eizaguirre & Santisteban, 2007).

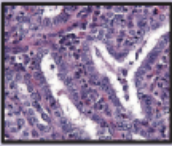
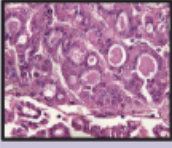
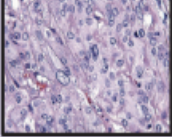
	Histology	Incidence	Driver genes	Survival rate	Other features
PTC		80%	BRAF ^{V600E} RET/PTC	95%	<ul style="list-style-type: none"> • Local spreading • Lymph node metastases • Low mutational burden
FTC		10-15%	RAS PAX8/PPAR γ	91%	<ul style="list-style-type: none"> • Haematological spreading • Bone and lung metastases • Low mutational burden
ATC		1-2%	BRAF ^{V600E} RAS PIK3CA PTEN	1-7%	<ul style="list-style-type: none"> • Locoregional invasion • Bone and lung metastases • High mutational burden

Figure 3 | Genetic and clinicopathological features of thyroid carcinomas. The main features of the most representative types of thyroid carcinomas, including PTC, FTC and ATC are shown. 40x magnification of histological sections are stained with hematoxylin and eosin. The ‘driver genes’ column shows the most frequent mutations associated with each type of thyroid carcinoma. The ‘survival rate’

column shows the 5-year overall survival rate. Figure adapted from Zaballos & Santisteban (2017).

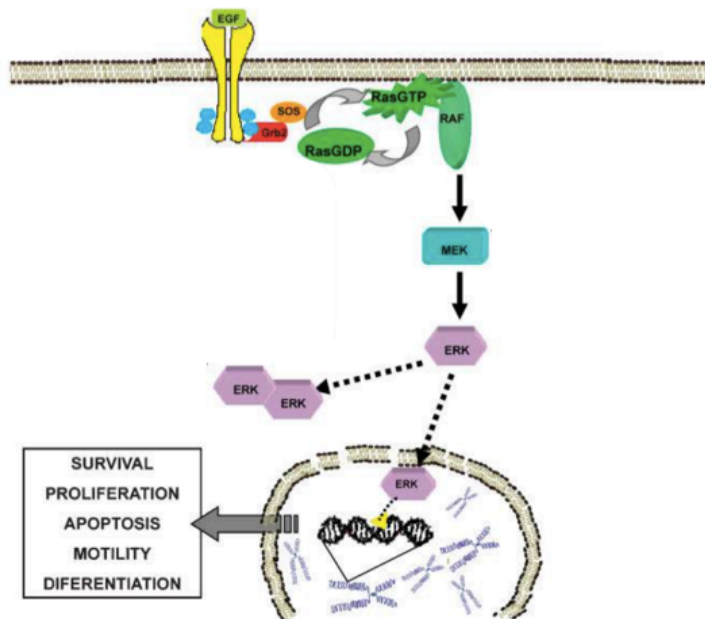
Treatment of thyroid cancer is mostly based on total thyroidectomy, ablative doses of radioactive iodine and suppressive treatments. Although, conventional treatments are advantageous for mostly thyroid cancers, novel effective therapies against those untreatable tumors need be developed. There are usually <10% of WDTC, many MTC and almost all ATC (Naoum et al., 2018). A vast body of data shows that the Ras-ERK pathway is involved in the control of homeostasis, the expression of cytokines and proteases, the progression of cell cycle, cell adherence, motility and metabolism being implicated in growth and survival of thyroid human tumor. Therefore, one option can be use therapeutic agents that suppress the oncogenic signaling through the Ras-ERK axis (Riesco-Eizaguirre & Santisteban, 2007).

1.2 THE RAS-ERK PATHWAY

The Ras-Raf-MEK-ERK (Ras-ERK) pathway is one of the well-defined MAPK cascades. This signaling cascade is able to carry an extensive variety of extracellular signals into control of cell proliferation, differentiation, migration, senescence and death in mammalian cells (O. Shaul, 1996). The pathway is compound by Ras, a small GTPase, three protein kinases: Raf, a MAPK kinase kinase, MEK, a MAPK kinase and ERK, a MAPK, and their phosphatases (Figure 4). The Ras-ERK cascade functions downstream of cell surface and it is activated in response to various extracellular stimuli like growth factors, antigen, chemokine or cytokines, which stimulate cell surface receptors such as tyrosine kinases, integrins and G proteins-coupled receptors. Furthermore, aberrant regulation of the MAPK cascade contribute to cancer and other human diseases (O. Shaul, 1996; Roberts & Der, 2007).

Figure 4 | The Ras-ERK signaling pathway A linear simplified representation of the Ras-Raf-MEK-ERK pathway.

Figure adapted from Calvo, Agudo-Ibáñez, & Crespo (2010).



The mammalian Ras protein family are composed by 3 isoforms: H-Ras, K-Ras (4A and 4B) and N-Ras. They are small GTPases that act like a switch between an inactive

state, when are bound to GDP, and an active state, when are bound to GTP. The change between these states is catalyzed by two proteins family: the guanidine exchange factors (GEFs), that promote the activation of Ras, and the GTPases activating proteins (GAPs), that stimulate the intrinsic Ras GTPase activity (Fey, Matallanas, Rauch, Rukhlenko, & Kholodenko, 2016). Ras proteins are typically associated with the inner layer of the plasma membrane (PM), but actually they present on a variety of intracellular membrane sub-localizations depends of the Ras isoform: endosomes, the Golgi complex (GC) and the endoplasmic reticulum (ER). Hence, Ras sub-localization can affect which effector pathway are activated and how intensively (Calvo, Agudo-Ibáñez, & Crespo, 2010). Classical activation happens from the interaction between growth factors with tyrosine kinase receptor, that result in receptor dimerization, activation and transphosphorylation. This activation recruit GEFs to the cell membrane and trigger Ras signal (Roberts & Der, 2007).

The next component downstream of Ras in this pathway is Raf kinase. The mammalian Raf protein family are composed by 3 isoforms: A-Raf, B-Raf and C-Raf, also called Raf-1. They are cytoplasmic three serine/threonine-specific protein kinases (MAPKKK) that need to be recruit into the PM and interact with GTP-bound Ras for their phosphorylation/dephosphorylation, dimerization, and association with scaffolding complexes (Neuzillet et al., 2014). Once Raf is phosphorylated and activated, it can activate the next component of Ras-ERK cascade, MEK family proteins, that are directly activate through phosphorylation (Fey, Matallanas, Rauch, Rukhlenko, & Kholodenko, 2016). These protein family are compound by MEK1 and MEK2, two cytoplasmic tyrosine and serine/threonine dual-specificity kinases (MAPKK) that can phosphorylate and activate ERK proteins, the last component of the Ras-ERK pathway. They are cytoplasmic serine/threonine-specific protein kinases (MAPK) which present two isoforms:

ERK1 and ERK2. After their activation, ERK can act in the nucleus, mainly like a monomer, or in the cytoplasm, for which is necessary that ERK dimerizes (Herrero & Crespo, 2016). Once activating, they can trigger a wide variety of nuclear and cytoplasmic targets (<600), including transcription factors, kinases, phosphatases and cytoskeletal proteins (Neuzillet et al., 2014).

Likewise, the signaling cascade downstream of extracellular stimulation can be simplify in $\text{RasGDP} \rightleftharpoons \text{RasGTP} \rightarrow \text{Raf} \rightarrow \text{MEK1/2} \rightarrow \text{ERK1/2}$. It is important to highlight that although Ras-Raf-MEK-ERK cascade has been described as a simple linear and unidirectional pathway of protein kinases, there are various associated proteins that form a complex signaling network (Roberts & Der, 2007). Ras may cross-talk with different signalling pathways, such as the PtdIns-3 kinase (PI3K), some protein family members that regulate survival, Rac and Rho proteins, associated with the regulation of the cytoskeleton and invasiveness of tumor cell, p38 MAPK, and c-Jun N-terminal (JNK) pathway, the stress-activated protein kinase pathway (Fey, Matallanas, Rauch, Rukhlenko, & Kholodenko, 2016; Mccubrey et al., 2012).

1.2.1 SUBLOCALIZATIONS OF RAS

As mentioned before, Ras proteins interact with different types of membranes and can anchor to different micro-domains. This is possible because, although the N-terminal domains contribute to membrane binding, the Ras C-terminal 22–25 amino acids of the HVR (hypervariable region) are sequences where direct post-translational take place processing Ras and allowing PM anchoring (Figure 5). In this region harbors the CAAX box where C is cysteine, A is aliphatic amino acid, and X is serine/methionine (Hancock & Parton, 2005). Right after its synthesis in the cytosol, Ras is rapidly farnesylated at the Cys186 within the CAAX box and associate with the ER. Now, this sequence can be proteolyzed and carboxymethylated, what allows Ras association with endosomes. Ras proteins are further modified with one or two palmitates, what also change the association of Ras from the GC to the PM. At the PM, Ras isoforms interact with distinct microdomains with different biochemical compositions and physical-chemical properties: disordered membrane (DM) and lipid rafts (LR) (a highly ordered, high density structure which is rich in cholesterol and saturated lipids) (Figure 6). The balance between PM sub-localization is due to palmitoylation and depalmitoylation processes, so Ras diffusion between different PM types requires changes in acylation. In cells exhibiting high levels of palmitoylation, Ras is located in DM. By contrast, in cells in which Ras is low palmitoylated, it is found in LR. Palmitoylation process is rapidly reversible, thus Ras undergo a palmitoylation/depalmitoylation cycle, whereby palmitoylated forms at the PM are released following depalmitoylation, and return to the GC, via retrograde transport (Figure 7). (Agudo-Ibáñez, Herrero, Barbacid, & Crespo, 2015; Calvo, Agudo-Ibáñez, & Crespo, 2010; Fehrenbacher, Bar-Sagi, & Philips, 2009).

Figure 5 | Membrane anchors of Ras proteins.

The fully processed C-terminal membrane anchors of H-, N- and K-Ras are represented in the upper image. The C-terminal cysteine residue of all Ras is farnesylated and carboxylmethylated (red) as a result of modifications directed by the C-terminal CAAX motif. The anchor of N- and H-Ras is completed by palmitoylation (blue) of one or two cysteine residues, and of K-Ras by a sequence of lysine residues (blue). The anchor, shown in grey in the lower image, is connected to the G-domain, >95% conserved between Ras isoforms, by the linker sequence of the HVR (shown in black). Figure from Hancock & Parton (2005).

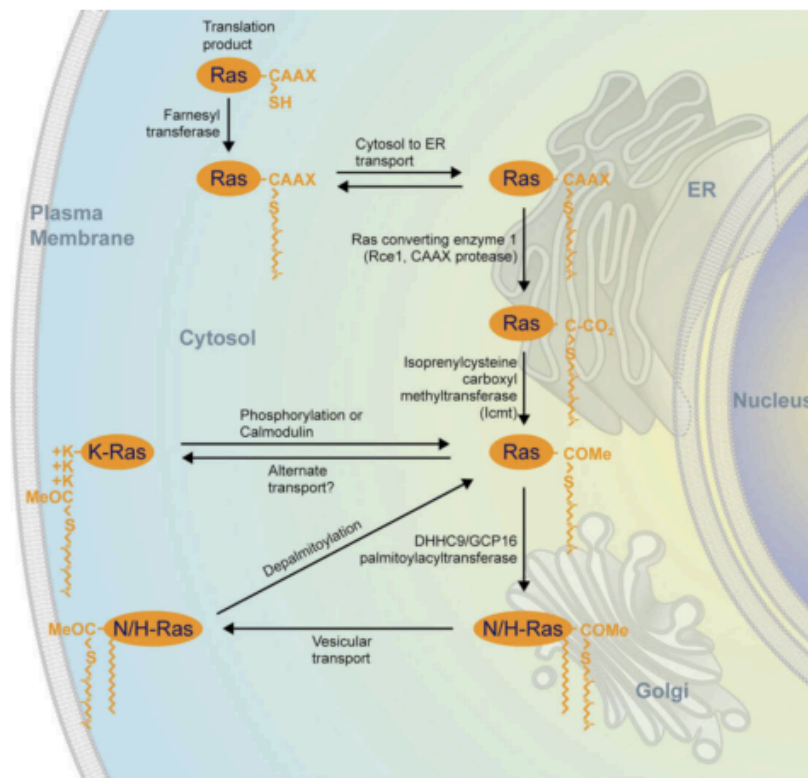
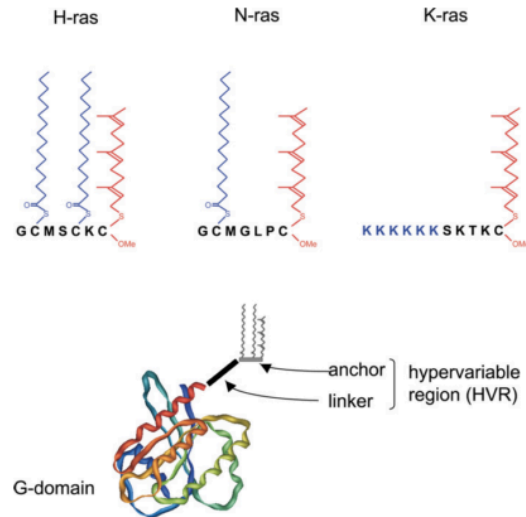


Figure 6 | Trafficking and post-translational modification of Ras. Ras is synthesized in the cytosol where CAAX box is farnesylated and Ras is sent to the ER. Here, it encounters Ras converting enzyme (Rce1) and isoprenylcysteine carboxyl methyltransferase (Icmt) that subsequently remove the AAX amino acids and methyl esterify the α carboxyl group. Then, K-Ras travel directly to the PM, while N- and H-Ras is sent to the GC, where they are modified with one or two palmitates to be sent to the PM. Both N- and H-Ras can be depalmitoylated and return to the GC, and K-Ras recycles back to endomembranes as a consequence of phosphorylation by PKC. From Fehrenbacher, Bar-Sagi and Philips (2009).

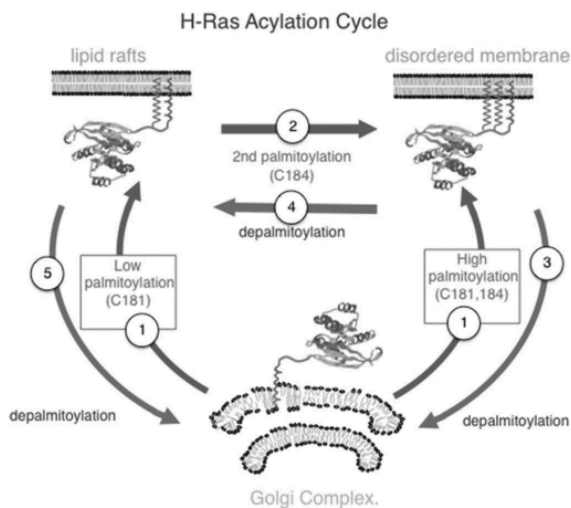


Figure 7 | H-Ras acylation cycle. H-Ras is palmitoylated at the GC and traffics to the PM through the exocytic route (1), occupy LR if it is monopalmitoylated in Cys181 or DM if it is bipalmitoylated in Cys181 and Cys184. Therein it can be totally depalmitoylated and traffic back to the GC via a non-vesicular route (3, 5). H-Ras can move inside the PM domains through a second palmitoylation in Cys184, that forces H-Ras to drift to DM (2), or a monodepalmitoylation in Cys184 that forces H-Ras to drift to LR (4). Figure from Agudo-Ibáñez et al., (2015)

A consequence of the Ras site-specific is a remarkable variability in its signal outputs. Whilst Ras activation at the PM is rapid and transitory, at the endomembranes is slow and constant (Calvo et al., 2010). Moreover, there are some differences in the levels of targeted Ras proteins present at the diverse domains, which may be due to the different types of membranes. So, using a targeted Ras approach as indicated in Matallanas *et al.* (2006), it is observed that ERK is preferably activated by ER-Ras signal, followed by LR and DM-Ras signal and, by last, lower levels of activation are found by GC-Ras signal. The Akt activation is signal is most efficiently stimulated in ER and LR, while Ral-GDS is preferentially activated at the GC. Finally, the JNK is activated with high intensity when Ras is tethered to ER and GC. Therefore, ER-Ras and DM-Ras were found to be essential of stimulating transformation, proliferation and survival, despite of GC-Ras and LR-Ras were absolutely dispensable for stimulating these responses (Calvo, Agudo-Ibáñez, & Crespo, 2010; Matallanas et al., 2006).

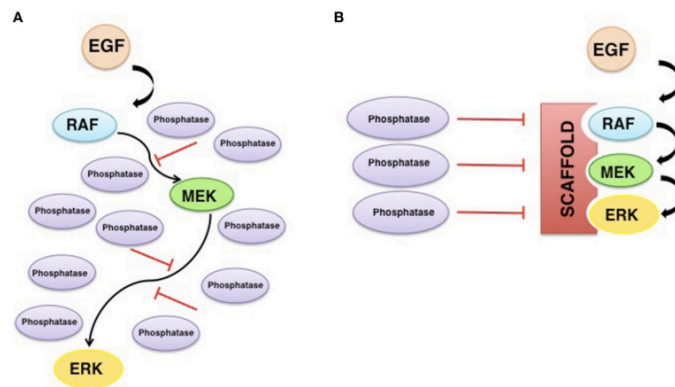
1.2.2 SCAFFOLDS OF THE RAS-ERK PATHWAY

Moreover, Ras-ERK pathway signals are not only the result of the diverse phospho-transfer reactions, but they are modulated by multiple regulatory proteins that acting at different stages of the cascade. These are known like scaffold proteins that connect the different members of the signaling cascade into a multienzymatic complex by which signal amplitude, intensity, spatial specificity and duration are fine-tuned (Figure 8). In addition, scaffold proteins provide signal fidelity through sequestering the signaling complex, thus preventing undesired molecular interferences. Their function optimize signaling based on tethering the proteins, increasing the optimal concentrations and orienting each protein to improve the phospho-transfer reactions and acting as allosteric stimulators to lift signal flux. Moreover, each scaffold protein act in different domains, activating site-specific ERK targets (Calvo, Agudo-Ibáñez, & Crespo, 2010; Casar &

Crespo, 2016). This shows the importance of protein-protein interactions and the spatial selectivity of ERK signals so that its activation occurs and spreads.

Figure 8 | Role of scaffold proteins in the Ras-ERK cascade.

Scaffolds promotes signal amplification: (A) When there are no scaffold proteins, the signal will be strongly down-regulated by phosphatases; (B) When there are scaffolds, the signaling is facilitating and enhancing and they shield proteins from dephosphorylation. Figure from Casar & Crespo (2016).



One family of MAPK scaffolds is the IQ motif-containing GTPase activating protein (IQGAP), a class of multidomain proteins, which are present in diverse organisms. Mammals express three isoforms: IQGAP1, IQGAP2 and IQGAP3, that have similar domain composition (Smith, Hedman, & Sacks, 2015). It has been recently demonstrated that blocking the interaction between the scaffold IQGAP1 and ERK, it is selectively inhibited tumors driven by Ras-ERK pathway oncogenes. By contrast, the absence of the scaffold IQGAP2 predisposes to development of hepatocellular, prostate and gastric carcinoma, suggest that it act as a tumor suppressor. Last, it has been seen that IQGAP3 enhances ERK phosphorylation following treatment with EGF and its overexpression promoted tumor cell growth migration and invasion (Casar & Crespo, 2016; Smith, Hedman, & Sacks, 2015). The binding properties of the IQGAPs motifs permit that interact with many partners and form multiple signaling complexes to regulate cellular processes such as cytokinesis, cell migration, cell proliferation, intracellular signaling, vesicle trafficking and cytoskeletal dynamics.

The IQGAP proteins share a similar domain structure and have considerable sequence homology. They contain several domains, namely a calponin homology domain (CHD), IQ region, WW domain, Ras GTPase-activating protein-related domain (GRD) and RasGAP_C-terminus (RGCT) (Figure 9). However, even if all the domains of IQGAPs are in several proteins, in IQGAPs they have exclusive characteristics. F-actin can associate with de CHD in numerous other actin-binding proteins, forms a high affinity interaction via tandem CHDs. Although, IQGAP1 only need a single CHD. Moreover, this domain can associate with calmodulin and Ca²⁺, which it is not common. The IQ motifs usually bind to IQ binding partners and, unexpected, in IQGAP1, they associate with EGFR, MEK or Rap1. While the WW domains bind to typically proline-rich regions in the binding partner. Nevertheless, in IQGAP1, it interacts with proteins that do not have a proline-rich region, like ERK. Moreover, the IQGAP GRD binds to and

stabilize small G-proteins in GTP-bound state. This is possible because this domain has a threonine instead of an arginine at a conserved catalytic residue, like occurs in GAPs. Finally, the RGCT is a domain unique to IQGAPs and can interact with other molecules. Additionally, the C-terminus can associate with other targets (Smith, Hedman, & Sacks, 2015).

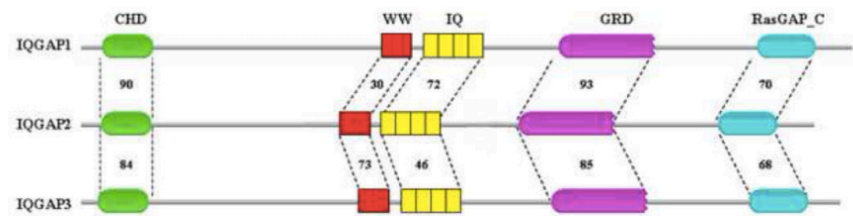


Figure 9 | Scheme of principles domains of human IQGAP proteins. Percentage amino acid identity between the IQGAP domains. CHD: calponin homology domain; WW: poly-proline protein-protein domain; IQ: IQ region (with four IQ motifs); GRD: Ras GTPase-activating protein-related domain; RasGAP_C: carboxy-terminal sequence. Figure from White, Brown, & Sacks (2009).

Multiple proteins interact to these domains and regulate diverse cellular processes, including cell migration, cell proliferation, vesicle trafficking, cytokinesis, intracellular signaling and cytoskeletal dynamics. mRNA expression of IQGAP2 was analyzed in order to find out differences between tumor and normal tissue, in multiple cancers (Figure 10) (Kumar, Hassan, Pattnaik, Mohapatra & Dixit, 2017).

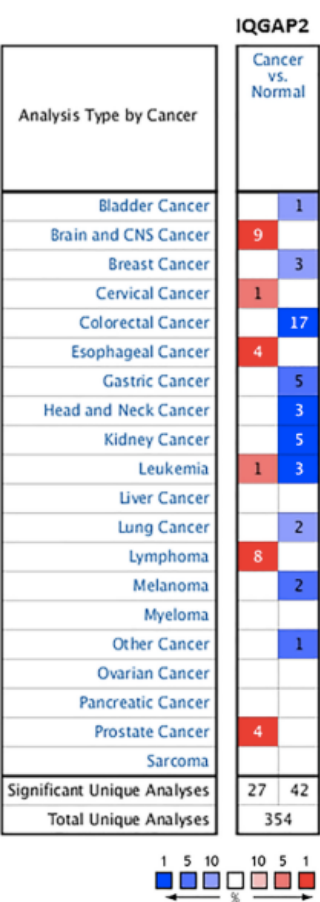


Figure 10 | The mRNA expression patterns of IQGAP2 in cancers. The mRNA expression difference, between tumors and normal tissues, were analysed in Oncomine database with thresholds of p-value<0.01, fold change>2 fold, gene rank <10%. The numbers in the colored cell represent the number of analyses meeting these thresholds. The red cells indicate increased mRNA expression whereas blue cells indicate reduced mRNA expression in tumor tissues, than in normal tissues. The color depth represents the gene rank, darker color shows better percentile for the analysis within the colored cell. Figure from Kumar, Hassan, Pattnaik, Mohapatra & Dixit (2017).

It has been seen that IQGAP2 is 62% identical to IQGAP1, differing in tissue distribution, subcellular localization and interaction with binding proteins. Thus, IQGAP2 is found predominantly in liver, but can also be detected in prostate, kidney, thyroid, stomach, testis, platelets and salivary glands (White, Brown, & Sacks, 2009). Some authors have demonstrated that IQGAP2 expression is downregulated in more invasive and metastatic liver cancer cell lines and also in a wide number of human hepatocellular carcinomas. Additionally, the promoter of IQGAP2 is methylated, decreasing IQGAP2 protein expression, in a vast majority cancer cells and this is significantly associated with tumor invasion and a poor prognosis (White et al., 2010). Thus, IQGAP2 expression is reduced in some neoplasms, but the changes are less consistent and not as well documented as the other members of its family being necessary further work to elucidate its role in human malignancies.

1.3 PROGRESS IN THE PIERO CRESPO'S LAB

Knowing and connecting all of these data, Piero Crespo's group and others started to investigate the roles of Ras-ERK pathway in thyroid tumorigenesis. Studies of thyroid biology are now developed *in vitro* due to the difficulties to obtain animals for experimentation and its controversial ethical and the simplicity and accessibility of cell lines. Thus, to achieve this aim, they used PCCL3 that it is a wild type cell line that was spontaneously immortalize and derives from rat follicular cells. These cells have been used extensively to explore the effects of oncogene activation on thyroid cells *in vitro* due to that any untransformed cell line from human origin has yet been established successfully (Kimura et al., 2001). Moreover, the high frequency of RAS mutations in follicular adenomas suggests a role for aberrant RAS activation as an early event in thyroid tumorigenesis. Interestingly, oncogenic RAS expression in PCCL3 cells induces genomic instability that could favor the accumulation of additional mutations, allowing progression to advanced thyroid carcinomas. Altogether, these findings suggest that RAS mutations predispose to malignancy and progression to aggressive undifferentiated tumors (Zaballos & Santisteban, 2017).

As it has been seen, the distinct site-specific Ras sub-signals participate in different ways in cellular transformation, in different types of cells, like it has been explained previously. However, in this type of cells had been untested thus far. For this purpose, Piero's group investigated the participation in the transformation process of ectopic H-Ras-V12 in PCC13 cells when selectively tethered to defined subcellular compartments by specific localization signals, like it was detailed in Matallanas *et al.* (2006): the avian infectious bronchitis virus M1 protein (for ER localization); the LCK myristoylation signal (for LR anchoring); the CD8 transmembrane domain (for DM localization); and the KDEL receptor N193D mutant (for GC localization). To activate H-Ras precisely at, and only at, the desired subcellular localizations, at Piero's laboratory were generated

constructs that encoded for constitutively active H-RasV12 fused to these specific tethering signals. It was used a palmitoylation-deficient H-RasV12 by mutating cysteines 181 and 184 to serines (H-RasV12 SS), where the palmitoylation signal was then substituted by the alternative cues that would specifically direct H-RasV12 SS to the desired locations. Moreover, an HA tag was included to be able to identify these proteins (Figure 11).

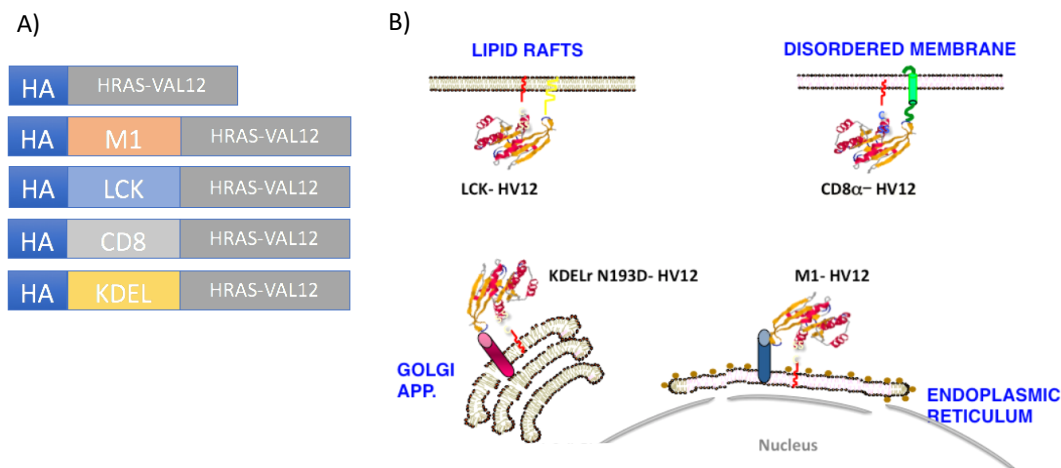


Figure 11 | A) Scheme of the H-RasV12 constructs to tethered H-Ras to the desired locations. Construct are formed for the HA tag, the specific localization signals (M1 to ER, LCK to LR, CD8 to DM and KDELr to GC) and the oncogenic H-RasV12. **B) Distribution of the site-specific H-RasV12 in the cell.**

To study a strategy for refining the inhibition of Ras-ERK signals in thyroid cancer, they analyzed whether scaffold proteins play different roles, depending on the sublocalization from which the aberrant signal emanates, using the already generated PCCL3 stable cell lines with the site-specific H-RasV12 constructs. Since scaffolds serve as dimerization platforms, Piero's group proceeded to study how the absence of specific scaffold proteins affects the oncogenic drive exerted by each oncoprotein. To this end, they utilized a battery of siRNAs, among which was the siRNA against IQGAP2.

The experiments described above aim at establishing how IQGAP2 scaffold protein participate in the different processes necessary for cellular transformation and the acquisition of migrative and invasive properties in cultured cells. Cancer cells could acquire these properties *in vivo* and develop metastasis, a complex process that occur when cancer spreads to another part of the body. It includes several steps: neoplastic, progression, angiogenesis, cell migration and invasion, intravasation into nearby blood vessels, survival in the circulatory system, extravasation and homing into distant tissues, the formation of micrometastases and growth into macroscopic secondary tumors (Crespo & Casar, 2016). It is difficult to study the metastatic process in animal models, but at Piero's laboratory they use a chick chorioallantoic membrane embryo model that

makes easier and faster to investigate and quantify tumor growth, invasion and metastasis an *in vivo* model. The chorioallantoic membrane (CAM), an accessible well-vascularized extra-embryonic tissue located under the eggshell, is receptive to xenografting mammalian tumor cells. The CAM can support the engraftment of tumor cells and faithfully recapitulates most of the characteristic of the carcinogenic process (Figure 12). Besides, the use of quantitative PCR allows the monitoring and quantification of the xenografted, ectopic tumor cells in distant tissues using specific primers for highly conserved specie-specific sequences (Crespo & Casar, 2016).

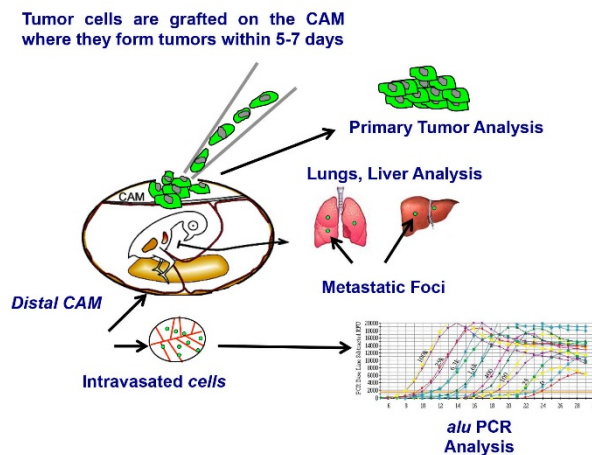


Figure 12 | Scheme of the spontaneous metastasis in chick embryo model. After 10 days of egg incubation, the CAM is dropped using a vacuum based system and tumor cells are put on the top of the CAM. Then, after tumor cells grow for 5-7 days, the tumor and chicken tissues are harvested for PCR analysis. Figure from Crespo & Casar (2016).

2. OBJECTIVES

Due to in this work I will be working with the already generated PCCL3 stable cell lines with the site-specific H-RasV12 constructs.

The first objective is determined if these already generated PCCL3 stable cell lines (HA-M1-HRasV12, HA-LCK-HRasV12, HA-CD8-HRasV12 and HA-KDELr-HRasV12) are correctly transfected.

Then, and thanks to the previous results obtained at Piero's laboratory, our hypothesis is that IQGAP2 is a scaffold protein that works as a tumor suppressor through the Ras-ERK cascade in thyroid cancer. Thus, this project was focus in how tumor thyroid cells behave when IQGAP2 it is not expressed. From this hypothesis arise the following objectives:

- Generate IQGAP2 knock out PCCL3 stable cell lines by CRISPR/Cas9 mediate genome editing in the different already generated PCCL3 H-RasV12 site-specific tethered to ER, LR, DM and GC stable cells lines.
- Compare the proliferative, migratory and invasive behavior of PCCL3 and the different site-specific Ras localization PCCL3 H-RasV12 (M1, LCK, CD8, KDELr) to their respective IQGAP2 knock out partners.
- Determine if the behavior of IQGAP2 knock out cells in the chick embryo animal model is different from the PCCL3 H-RasV12 (M1, LCK, CD8, KDELr).

3. MATERIALS AND METHODS

Cell culture

PCCL3 cells and the different site-specific PCCL3 H-RasV12 (PCCL3 H-RasV12, PCCL3 H-RasV12 M1, PCCL3 H-RasV12 LCK, PCCL3 H-RasV12 CD8, PCCL3 H-RasV12 KDELr) cells was routinely maintained in the 6H medium containing 20µg/ml Gly-His-Lys acetate salt, 1µM hydrocortisone, 1µg/mL somatostatin, 500µg/mL apo-transferrin, 0,05U/mL thyrotrophic hormone (TSH), 1mg/mL insulin, and supplementing with 5% fetal call serum (FCS), 1% penicillin/streptomycin, 1% Non-Essential aminoacids and 1% L-glutamine. All the cells were maintained in an incubator at 37°C, with 5% of CO₂ and 98% of relative humidity.

Constructs and bacteria transformation

The expression vector was encoded to the CRISPR/Cas9 of IQGAP2 scaffold protein. The transformation of bacteria with the foreign DNA was performed through heat shock. *Escherichia coli* DH5α, competent cells, were taken out from -80°C and thawed on ice (4°C) 30 minutes. 4 ng of the DNA was put into 30µL of competent cells in a microcentrifuge tube it was then placed into a 42°C water bath for 60 secs. The tubes were put back into ice for 5 minutes and 1ml of SOC medium (Invitrogen) was added, without antibiotic, to the bacteria and grown in a 37°C shaking incubator for 1h. 200µL of transformed cells were incubated with 5mL of Luria Broth culture medium (LB) containing ampicillin (1mg/mL) by shaking overnight.

Plasmid DNA isolation

Small scale purification of plasmid DNA was carried out from bacterial cultures derived from transformed strains of *Escherichia coli* DH5α. Bacterial cultures were grown in a total volume of 5 mL of LB for 12 hours, at a temperature of 37°C in the presence of ampicillin, the selection antibiotic to the resistance provided by the plasmid. After that period, following the instructions recommended by Thermo Fisher Scientific, manufacturer of the GeneJet Plasmid miniprep kit, it was centrifuged at 13000 rpm for 4 minutes. By pulling the supernatant, the pellet was resuspended in 250µL of Resuspension Solution, then smoothed for one minute, and 250µL of Lysis Solution was added and properly mixed. After that it was neutralized by adding 350µL of Neutralization Solution and mixed again by inverting the tube. Then, after having centrifuged at 13000 rpm for 5 minutes, the supernatant was passed through the exchange column, over which a series of washes are carried out with a mixture of washing solution with ethanol. Finally, the DNA was eluted using 50µL of Elution Solution and stored at -20°C, for later use for transfection. DNA concentration was checked with an agarose gel containing 0.5µg/ml of ethidium bromide in TAE buffer (0.09 M Tris-acetate, 2mM EDTA). Loading buffer (0.005 % (w/v) of

bromophenol blue 2% and 30% (v/v) of glycerol 100%) was added to the samples that were charged and submitted to electrophoresis at 70V. λ Hind III was used a concentration reference (1 μ g/ μ L).

Transfection

Subconfluent cells were transfected by Lipofectamine LTX and Plus Reagent (Invitrogen) to generated stable cell lines that include the CRISPR/Cas9 IQGAP2 construct. These were transfected by following the manufacturer's guideline and the total amount of plasmid DNA was adjusted to 3 μ g per plate. DNA was diluted in Opti-MEM medium. LTX Reagent and Plus Reagent was diluted in Opti-MEM (LTX Mix). Both were incubated 5 minutes at room temperature. LTX Mix was added to the DNA and incubated 10 minutes at room temperature. The cells were washed with phosphate-buffered saline (PBS) 1X and the mixture was added. After that cells were completed with 6H medium and next morning medium was changed.

Antibodies

The antibodies used during this project were shown in the table 1.

Antibody	Specificity	Dilution	Origin
Anti-IQGAP2	Mouse monoclonal	1:1000	Sta. Cruz Biotechnology (Ref. Sc-17835)
Anti-P-ERK	Rabbit polyclonal	1:1000	Sta. Cruz Biotechnology (Ref. Sc-7383)
Anti- α -tubulin	Mouse monoclonal	1:1000	Sigma-Aldrich (Ref. T6199)
Anti-hemagglutinin	Rabbit polyclonal	1:100	Sta. Cruz Biotechnology (Ref. Sc-805;
Anti-calreticulin	Mouse monoclonal	1:100	BD Biosciences Pharmingen (Ref. 612136)
Anti-GM130	Mouse monoclonal	1:100	BD Biosciences Pharmingen (Ref. 610822).
Anti- Na ⁺ /K ⁺ -ATPase	Mouse monoclonal	1:400	Upstate Biotechnology Inc. (Ref. 05-369)

Table 1 | List of antibodies which were used during this project.

Immunofluorescence

The different site-specific PCCL3 H-RasV12 cells were grown in sterile glass coverslip (10mm diameter) until they achieved subconfluent density. All cell lines were washed two times in PBS 1X in order to remove any residual media and were fixed with 4% paraformaldehyde. Preparations were sequentially incubated in 0.1M glycine-PBS for 5 minutes and washed in PBS 1X (3x5 minutes). Then cells were hatched with PBS–0.01% Tween 20 for 5 minutes and washed in PBS 1X (3x5 minutes). In all cases, preparations were incubated with the pertinent primary antibodies listed before overnight in a high humidity room at 4°C, washed in PBS 1X (3x5 minutes), and incubated with secondary antibodies conjugated to Alexa Fluor 594 and Alexa Fluor 488 for 1h in a high humidity room, at room temperature and darkness. Preparations were assembled in slides with Prolong Gold antifade reagent with DAPI H-1200 (Invitrogen). Images were taken in Axioimager (Carl Zeiss) microscope and the pictures were put together thanks to Fiji software.

Protein isolation

To obtain total extract of protein from the cell cultures, cells were put on ice and washed with PBS 1X to eliminate possible residues. Then, it was added 350µL of lysis buffer with high stringency that contains 20mM HEPES pH 7.5, 10mM EGTA, 40mM β-glycerolphosphate, 1% of non ionic detergent NP40, 2.5mM MgCl₂, 2mM orthovanadate, 1mM DTT (dithiothreitol), 1% de CHAPS, proteases inhibitor (10µg/mL aprotinin and 10µg/mL leupeptin) and 1mM PMSF. After 5 minutes, lysates were centrifugated at 13000 rpm 10 minutes at 4°C and supernatants were collected. To measure and set protein concentration the colorimetric method of Bradford with the DC™ (Detergent Compatible) Protein Assay kit from Bio-Rad was used. Then, it was added 25µL of mix of Protein Assay Reagent A and Proteins Assay Reagent S (50:1) and 200µL of Protein Assay Reagent B to 5µL of the total extract of protein. The mix was then incubated 10 minutes at 37°C and finally, it was measured absorbance at 620 nm with the spectrophotometer.

Immunoblotting

1X Laemmli buffer (100mM Tris pH 6.8, 4% SDS, 20% glycerol, 20mM DTT and 0.005% bromophenol blue) was added to the samples and were heated at 95°C 5 minutes. Samples were fractionated by an 8% sodium dodecyl sulfate-polyacrylamide gel electrophoresis (SDS-PAGE) in Mini-protean devices (Bio-Rad). Proteins were electrophoretically transferred to nitrocellulose membranes (Milipore) in 1% Tris-Glycine pH 8.4. Then, membranes were blocked in TBS-T buffer (Tris Buffer Saline-Tween 20: 20mM Tris pH 7.5, 137mM NaCl and 0.05 % de Tween 20) containing 4% of BSA (bovine serum albumin, SIGMA) for 1 hour at room temperature. The blots were incubated with the primary antibodies listed before (100µg/ml) in blocking solutions

overnight at 4°C shaking. Two washes were performed in TBS-T for 10 minutes each at room temperature shaking. Then, membranes were incubated 1h with horseradish peroxidase-conjugated secondary antibodies diluted 1:5000 in TBS-T buffer containing 4% milk powder at room temperature shaking. Then, two washes were performed in TBS-T for 10 minutes each at room temperature shaking. Immunocomplexes were visualized by enhanced chemiluminescence detection system (ECL™ kit from Amersham). To check if the protein concentration was equal, α -tubulin was analyzed using an anti- α -tubulin antibody. Membranes were autoradiography with Kónica-Minolta films.

Measurement of proliferation and survival rates

PCCL3, PCCL3 H-RasV12, PCCL3 H-RasV12 LCK, PCCL3 H-RasV12 KDElr and their respective cell line transfected with CRISPR/Cas9 IQGAP2 cells were plated at 30,000 cells/well density in 12-well plates and at 5,000 cells/well density in a 96-well plate and cell were counted in a Neubauer Chamber or using the PrestoBlue Cell Viability Reagent protocol from Invitrogen at different times (24, 48 and 72 hours). For this, 10 μ L of PrestoBlue™ Cell Viability Reagent was added to 90 μ L of media (control) or to cells+media. After 5h the absorbance was measured at 540nm (excitation) and 620nm (emission) with the spectrophotometer. To evaluate the results and statistical significance of experimental groups, Graph Pad Prism software was used using a Student T-test.

Measurement of cell migration

PCCL3, PCCL3 H-RasV12, PCCL3 H-RasV12 LCK, PCCL3 H-RasV12 KDElr and their CRISPR/Cas9 IQGAP2 respective cell lines were plated at 40,000 cells/well density in a 24-well plate with Transwell cell culture inserts adding 150 μ L of serum-free 6H media (without FBS) (Figure 13). In the down-compartment 500 μ L of 6H media containing 5% FBS. After 48h, pictures were taken using a Nikon DS-Fi2 microscope. To evaluate the results and statistical significance of experimental groups, Graph Pad Prism software was used using a Student T-test.

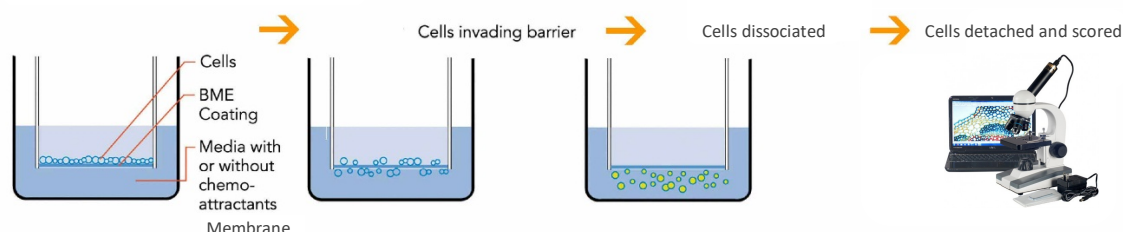


Figure 13 | Illustration of the cell migration protocol. Inside each well, a transwell, which is a cylindrical insert, is placed. The insert has an 8 μ m pore polycarbonate membrane. When placed in the well, it divides the chamber into two compartments and cells can move from the up to the down-compartment determining their migratory capacity. Figure adapted from Amsbio web site.

Measurement of cell invasion

PCCL3, PCCL3 H-RasV12, PCCL3 H-RasV12 LCK, PCCL3 H-RasV12 KDElr and their CRISPR/Cas9 IQGAP2 respective cell lines were plated at 40,000 cells/well density resuspended in 150 μ L of serum-free media in a 24-well plate with Transwell cell culture inserts previously covered with 50 μ L of matrigel resuspended on serum-free media (1:20). In the down-compartment was added 500 μ L of 6H media containing 5% FBS. After 72h, pictures were taken using a Nikon DS-Fi2 microscope. To evaluate the results and statistical significance of experimental groups, Graph Pad Prism software was used using a Student T-test.

Preparing tumor cells for grafting

IQGAP2 knock out PCCL3 H-RasV12, IQGAP2 knock out PCCL3 H-RasV12 LCK and IQGAP2 knock out PCCL3 H-RasV12 KDElr were washed in PBS 1X twice in order to remove any residual media and were detached from their culture dishes using trypsin/EDTA. Cells were counted using NucleoCounter (ChemoMetec) and were resuspended in serum-free 6H at 40 million cells/ml (10^6 cells/0,025 μ L).

Preparing the eggs for xenografting tumor cells

Freshly fertilized chicken eggs (Gibert Farm Tarragona, Spain) were incubated on their side in a incubator at 37 °C and 60% humidity rotating every 30 minutes for 10 days. On day 10, the eggs were placed on their side on an egg rack. The embryo was therefore located near the bottom of the egg and the air sack on its right. The area was cleaned using a cotton swab soaked with iodine and a small hole was drilled through the eggshell into the air sack using a 30-gauge syringe needle (Figure 14A). Another hole was done in the egg top, penetrating the shell membrane but not the CAM, using a Dremel rotary tool kit (Figure 14B). After, a 20-gauge syringe needle with a small hook on the end was used to make a third very small hole in the eggshell membrane (Figure 14C). To suction, a vacuum like system was created with an automatic pipette aid fitted with a piece of Tygon tubing placed against the hole in the airsac (Figure 14D). To separate the CAM from the shell and let it drop, a mild vacuum was applied to the hole over the air sack, so the blood vessel dropped down, away from the eggshell and attaches to the embryo. A pair of needle-nose forceps or the Dremel rotary tool kit was used do a square window (1 cm²) to expose the underlying CAM (Figure 14E). Then a 20-200 μ L pipette was used to place 25 μ L of the cell suspension onto a small area of the CAM (Figure 14F). The window in the egg was tightly closed with laboratory tape and eggs were leaved in a position with the embryos standing upright for 5-10 minutes, in order to allow the cells to settle. Then the eggs were settle in an egg rack into a stationary incubator at 37 °C and 60% humidity. Cells were allowed to grow for 7 days for a macroscopic tumor to be visible.

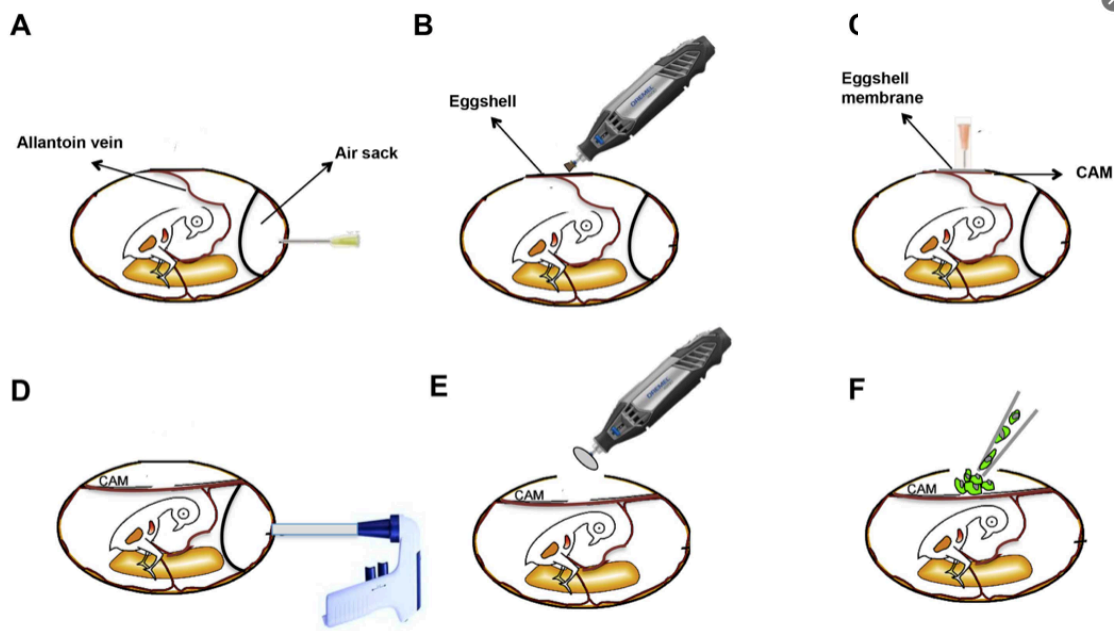


Figure 14 | Steps of the eggs preparation for xenografting tumor cells. Figure from Crespo & Casar (2016).

Harvesting tumors and chick embryo tissues and genomic DNA isolation

After 7 days for the insertion of tumor cells, it is opening a new window removing some eggshell until the tumors become visible. The primary tumor was resected from the CAM and weighed. The shell was cut radially to remove the chick embryo from the eggshell and the embryo was transferred to a clean weight boat. With a clean set of tools, the embryo was dissected, cutting through the sternum. Pieces of the liver and the lungs were collected. The distal CAM was resected from the eggshell in PBS 1X. The samples were incubated with 0.03% proteinase K lysis buffer (Qiagen) and disaggregated using the polytron. After, samples were incubated overnight at 65°C. The morning after 200µL of protein precipitation solution was added and a 13000 rpm centrifugation during 5 minutes was performed. Supernatant was recovered and mixed with isopropanol (1:1) letting it to settle for 5 minutes. After same centrifuged at 13000 rpm 5 minutes in order to get the genomic DNA. Then, the pellet was washed with 70% ethanol and a last centrifugation step was done at 13000 rpm for 5 minutes. Supernatant was then removed and pellet containing the genomic DNA was dried 5 minutes uncovered and resuspended in 200µL of hydration solution.

PCR analysis

30ng of genomic DNA was used as template in a 25µL reaction containing 12,5 µL of SYBR Select Master Mix (Applied Biosystems), 0.4µmol/L of each primers (Rat PCR Forward: 5'-

CAAAAATGGAGCTGCGCAG-3'; Rat PCR Reverse: 5'-CGCCAGCTGGTGGGGATT-3') and ultrapure water. The PCR was run under the following conditions: 95°C for 2 minutes, 40 cycles at 95°C for 30 seconds, 63°C for 30 seconds, 72°C for 30 seconds. A standard curve was generated using a dilution series of human DNA (10^2 , 10^3 , 10^4) from the original tumor cells and water was used as a negative control. Ct values were calculated in duplicate and they were extrapolated to the standard curve being able to calculate the number of tumor cells contained in CAM, lung and liver samples. To evaluate the results and statistical significance of control and experimental groups, Graph Pad Prism software was used using a Student T-test.

4. RESULTS

Selective tethering of H-RasV12 to defined sublocalizations in PCCL3 cells

The first objective was to determine where H-RasV12 was distributed when PCCL3 were transfected with the different constructs (HA-M1-HRasV12, HA-CD8-HRasV12 and HA-KDELr-HRasV12). For this purpose, we used a specific marker for the tag protein labeled to all H-RasV12 constructs that is (HA) and for the different domains: DM (Na^+/K^+ -ATPase), ER (Calreticulin) and GC (GM130). We could see that PCCL3 H-RasV12 (H-Ras) cells were correctly transfected and H-RasV12 was distributed as expected throughout the cell (Figure 15 A). In the same way, PCCL3 H-RasV12 KDELr (KDELr) were expressing H-RasV12 at the GC

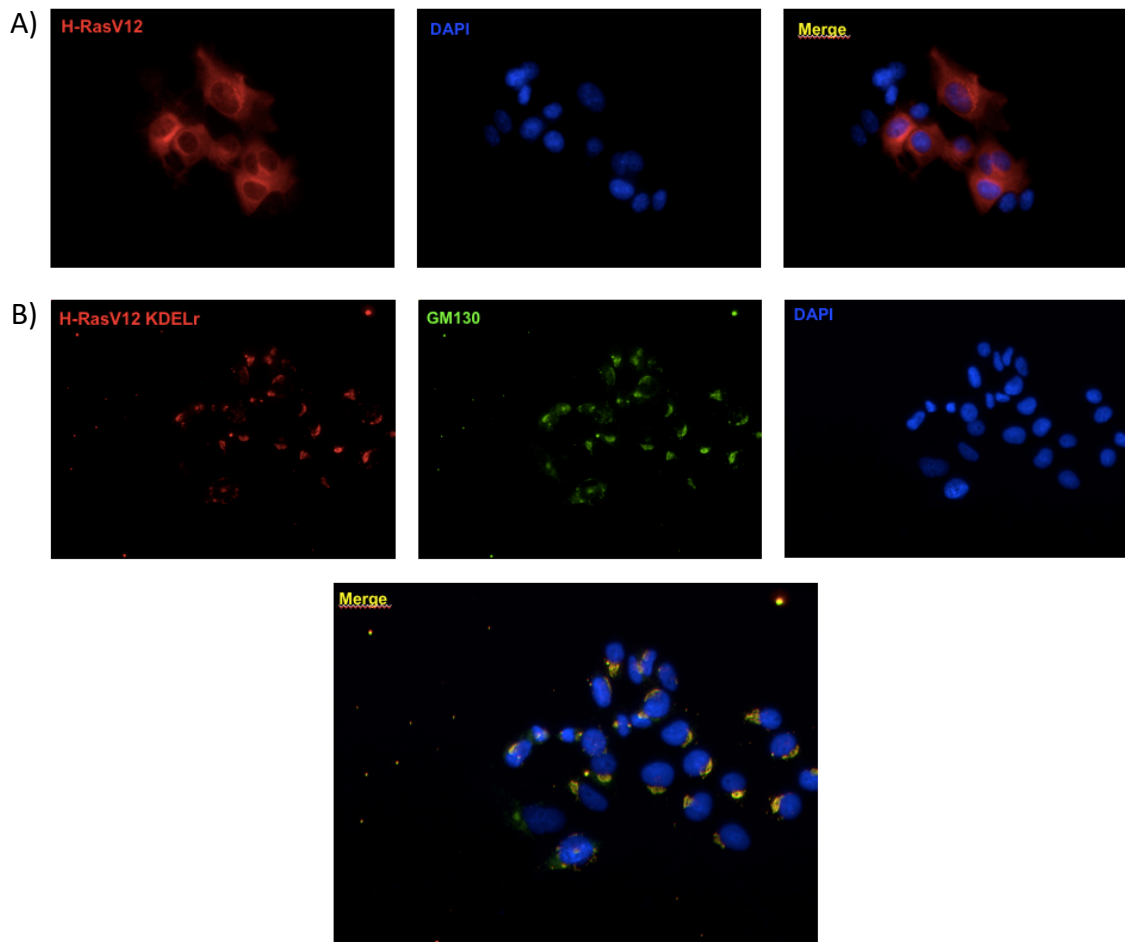


Figure 15 | Subcellular localization of targeted H-RasV12. **A)** Images (40X) of PCC3 cells stably transfected with the H-RasV12 construct, immunostained with anti-HA (red, first panel) and DAPI (blue, second panel). **B)** Images (20X) of PCC3 cells stably transfected with the HA-KDELr-HRasV12 construct. H-RasV12 proteins were revealed by anti-HA (red, first panel) costained with GM130 (green, second panel) as GC marker and the nucleus were revealed by DAPI (blue, third panel). Colocalization of HA-KDELr-H-RasV12 with the GC (Merge).

as it is shown in the figure co-localizing with the GC marker GM130 (Figure 15 B). However, the immunofluorescences for PCCL3 HRasV12 M1 (M1) and PCCL3 H-RasV12 CD8 (CD8) were performed although any clear images were able to be taken.

Down-regulating the expression of IQGAP2 in tumor thyroid cells

In order to achieve the second objective of analyze the role of IQGAP2 in thyroid cancer cells, we blocked the expression of IQGAP2 by CRISPR/Cas9 mediate genome editing in PCCL3 stable cell lines with the site-specific H-RasV12 constructs (HA-M1-HRasV12, HA-LCK-HRasV12, HA-CD8-HRasV12 and HA-KDELr-HRasV12). We only were able to obtain IQGAP2 knock out PCCL3, PCCL3 H-RasV12, PCCL3 H-RasV12 LCK (LCK) and KDELr cell lines as described in Material and Methods. To verify if the transfection was effective, we checked by Western blot the expression of IQGAP2 in the different cells lines (Figure 16).

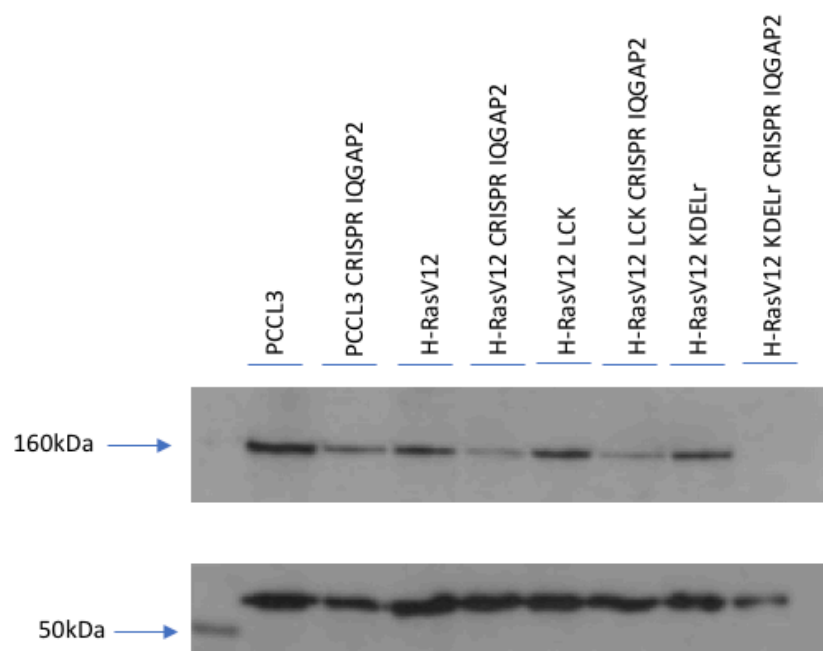


Figure 16 | Proof of IQGAP2 scaffold protein knock-out using CRISPR/Cas9 system in PCCL3 H-RasV12, H-RasV12 LCK and H-RasV12 KDELr stable cell lines. Cells were transfected with CRISPR/Cas9 IQGAP2 construct and were lysed. Then, the total protein was obtained and samples were fractionated by 8% SDS-PAGE and transferred onto nitrocellulose membranes as described in Material and Methods. All IQGAP2 knock out cell lines shown a dramatic reduction of IQGAP2 scaffold protein expression.

Moreover, we also checked the activation of ERK by Western blot in order to see if there were some differences as IQGAP2 is a scaffold protein that facilitates the phosphorylation of the different mediators of Ras-ERK signaling pathway. We then saw that the loss of IQGAP2 in

the PCCL3 WT cell line was able to dramatically reduce the levels of P-ERK. In striking contrast, the loss of IQGAP2 expression in H-Ras, LCK and KDELr was not able to reduce the levels of P-ERK suggesting that H-RasV12 mutated cells are not IQGAP2 dependent to perform its cellular activities (Figure 17).

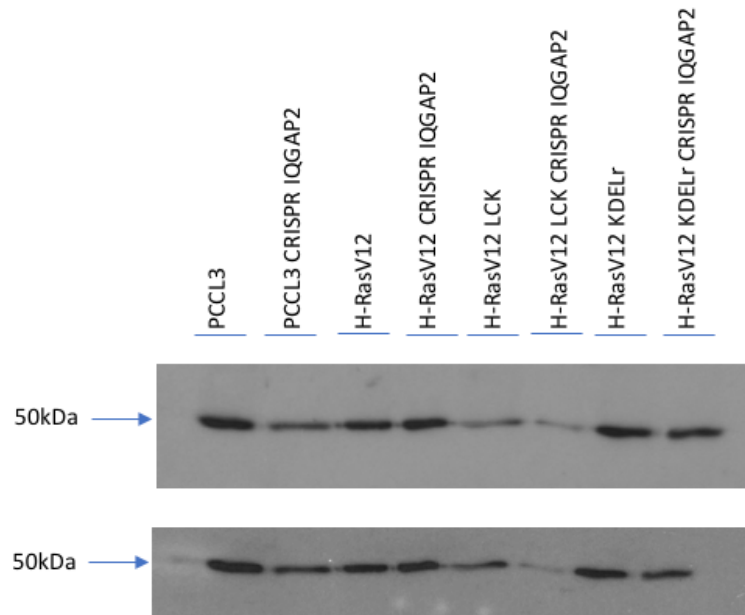


Figure 17 | P-ERK levels in PCCL3 H-RasV12, H-RasV12 LCK and H-RasV12 KDELr stable cell lines and their IQGAP2 CRISPR/Cas9 partners. Cells were transfected with CRISPR/Cas9 IQGAP2 construct and were lysed. Then, the total protein was obtained and the activation of P-ERK was analyzed by Western blot. IQGAP2 knock out PCCL3 cell line shown a clear reduction of the ERK phosphorylation levels. However, this reduction was not observed in the IQGAP2 knock out H-Ras, LCK and KDELr cell lines.

Proliferative behavior of tumor thyroid IQGAP2 knock out cells

To check if the down-expression of IQGAP2 in thyroid tumor cells was able to affect proliferation, we measured the cell growth at 24, 48 and 72 hours. For this purpose, we used two different methods: we first used a Neubauer chamber to count the number of cells and second, we measured their metabolic activity using Presto Blue as described above. Although we saw different proliferative behaviors depending of the PCCL3 cell line that we studied, the statistical analysis did not show significant differences (Figure 18)

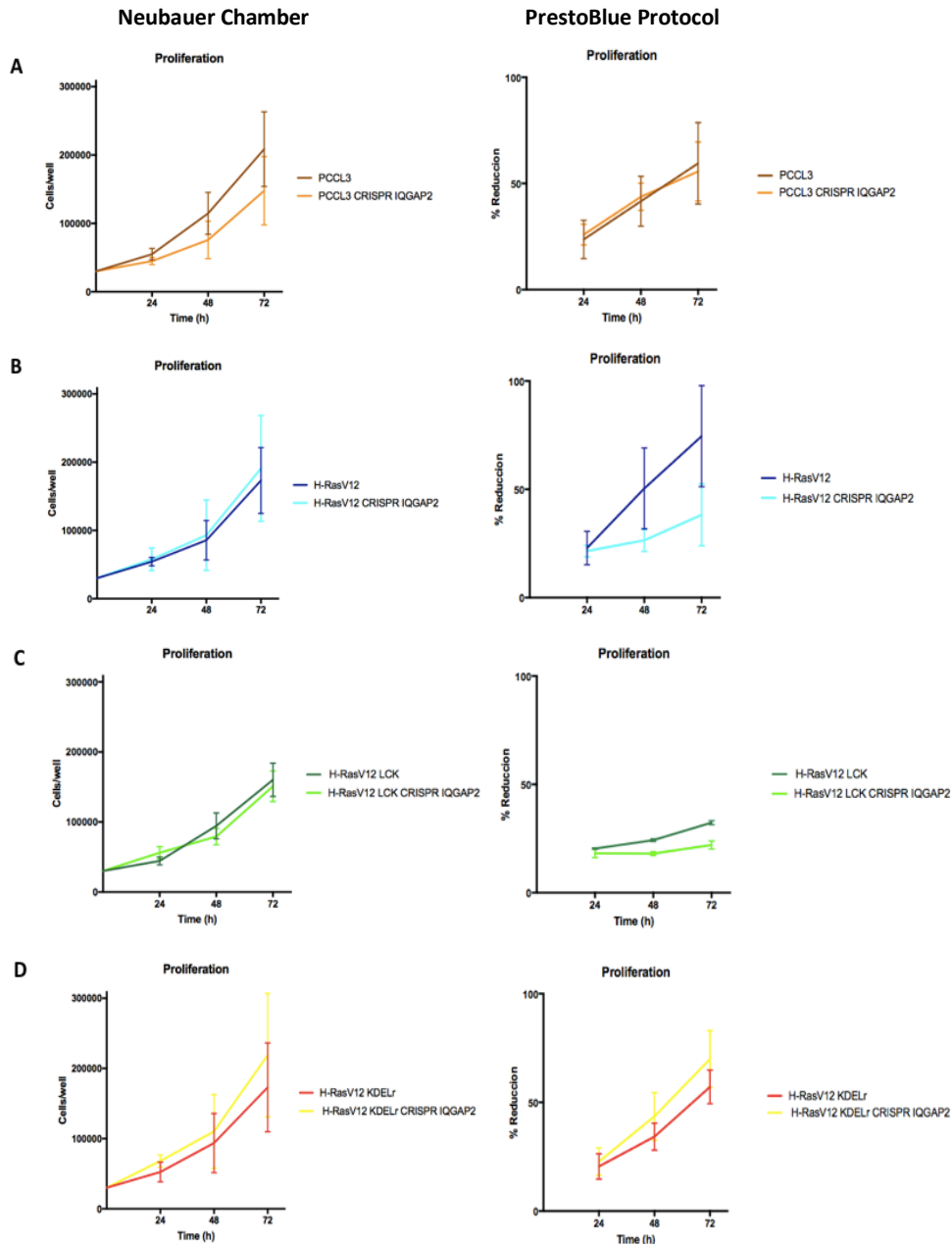


Figure 18 | Proliferation behavior of IQGAP2 knock out PCCL3 stable cell lines with the site-specific H-RasV12 constructs. Graphics show the number of cells (left) and the percentage of reduction of the Presto Blue reagent (right) at 24, 48 and 72 hours demonstrating its metabolic activity of the PCCL3(A), H-RasV12 (B), H-RasV12 LCK (C), H-RasV12 KDELr (D) and their IQGAP2 knock out partner cell lines. In all cases, results show the average \pm the standard error of the mean (SEM) and analysis of variance was performed by using the Student t-test.

Migratory behavior of tumor thyroid IQGAP2 knock out cells

To check if the down-expression of IQGAP2 in thyroid tumor cells were able to induce migration, we perform a Transwell assay where we saw that PCCL3, LCK and their IQGAP2 knock out partners were not able to migrate. However, in contrast, although H-Ras and KDELr

were able to migrate, their IQGAP2 knock out partners showed a significant increase demonstrating that IQGAP2 might be acting as a tumor suppressor by inhibiting or braking their migratory behavior (Figure 19).

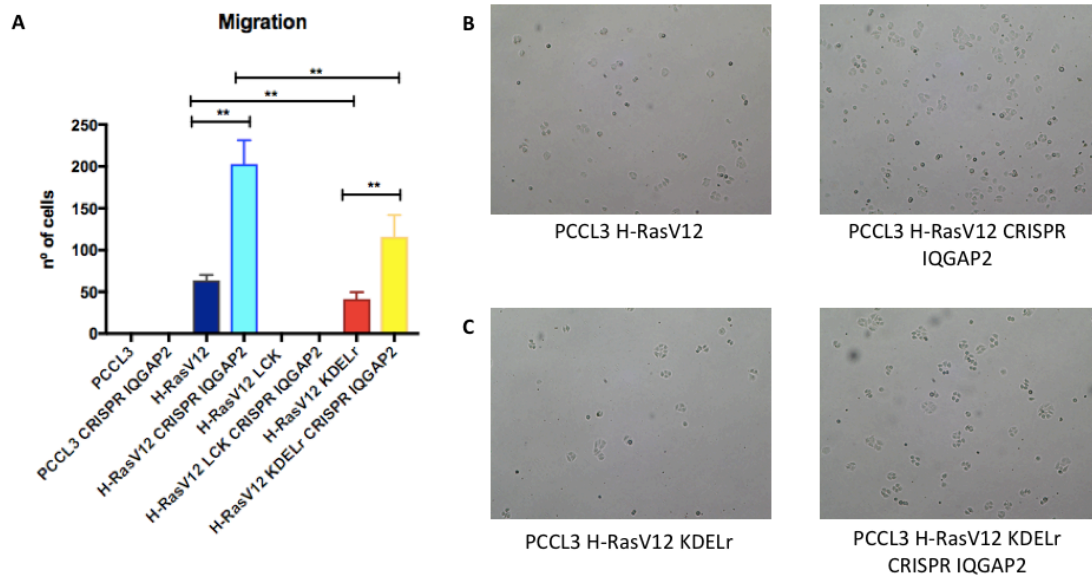


Figure 19 | Migratory behavior of IQGAP2 knock out PCCL3 stable cell lines with the site-specific H-RasV12 constructs. **A)** The graphic shows the number of PCCL3, H-RasV12, H-RasV12 LCK, H-RasV12 KDELr and their IQGAP2 knock out partners cells that were able to migrate through the 8 μ m pore polycarbonate membrane contained in Transwell cell culture inserts at 48 hours. The bar chart shows the average \pm the SEM and analysis of variance was performed by using the Student t-test. P-value: **, P-value<0.005. **B, C)** Images (10X) of PCCL3 H-RasV12 (left) and IQGAP2 knock out PCCL3 H-RasV12 (right) cells and PCCL3 H-RasV12 KDELr (left) and IQGAP2 knock out PCCL3 H-RasV12 KDELr (right) that were able to invade to the bottom of the plate at 72 hours using a Nikon DS-Fi2 microscope.

Invasive behavior of tumor thyroid IQGAP2 knock out cells

To check if the down-expression of IQGAP2 in thyroid tumor cells were able to induce invasion, we perform a Transwell assay using a Matrigel coating where we saw that PCCL3, LCK and their IQGAP2 knock out partners were not able to invade the down-compartment. We also saw that both H-Ras and its IQGAP2 knock out partner were able to invade it, but the statistical analysis did not show significant differences. However, although KDELr was able to invade the bottom, their IQGAP2 knock out partner showed a dramatic increase demonstrating that IQGAP2 might be acting as a tumor suppressor by inhibiting or braking their invasive behavior in this localization (Figure 20).

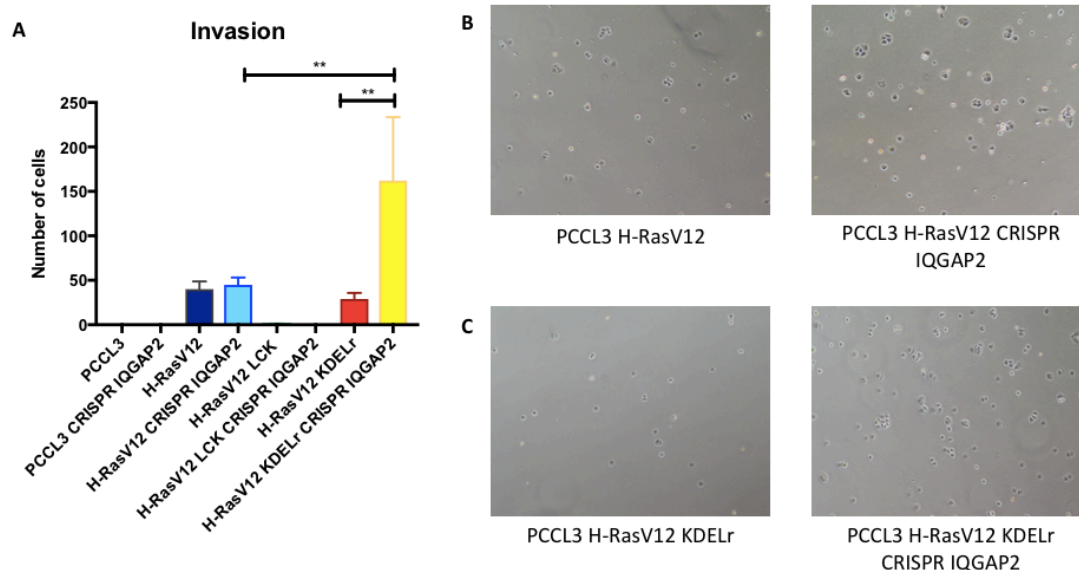


Figure 20 | Invasive behavior of IQGAP2 knock out PCCL3 stable cell lines with the site-specific H-RasV12 constructs. **A)** The graphic shows the number of PCCL3, H-RasV12, H-RasV12 LCK, H-RasV12 KDELr and their IQGAP2 knock out partners cells that were able to invade through the 8 μ m pore polycarbonate membrane contained in Transwell cell culture inserts previously covered by Matrigel at 72 hours. The bar chart shows the average \pm the SEM and analysis of variance was performed by using the Student t-test. P-value: **, P-value<0.005. **B, C)** Images (10X) of PCCL3 H-RasV12 (left) and IQGAP2 knock out PCCL3 H-RasV12 (right) cells and PCCL3 H-RasV12 KDELr (left) and IQGAP2 knock out PCCL3 H-RasV12 KDELr (right) that were able to invade to the bottom of the plate at 72 hours using a Nikon DS-Fi2 microscope.

Tumor Growth and Metastasis in Animals *in vivo*

Finally, to determine if the behavior of IQGAP2 knock out cells in the chick embryo animal model is different to the distinct IQGAP2 knock out PCCL3 lines (H-Ras, LCK and KDELr) we put 1.000.000 cells in chick embryos at day 10 of their development as described in Materials and Methods and seven days after tumors were harvested. As we expected, the vast majority of them presented a similar size, except IQGAP2 knock out KDELr that shown a significant increase of the tumor weight (Figure 21A). On the other hand, the samples of CAM, lungs and liver were analyzed to check if these cells were able to metastasize. IQGAP2 knock out H-Ras cells were able to migrate and extravasate specially to the CAM and, to a lesser extent, to the liver (Figure 21 B and D). On account of its cellular behavior, IQGAP2 knock out LCK should not be able to invade other tissues. However, in the chick embryo animal model these cells were able to migrate, in these cases, to the CAM and to the lungs, but not to the liver (Figure 21B and C). IQGAP2 knock out KDELr cells were able to migrate and extravasate all the tissue (Figure 21 B, C and D). Although our hypothesis was that IQGAP2 act as a tumor suppressor, unique significative

results were observed in KDELr cells. Hence, more studies with higher sample size might help providing a better perspective on the role of IQGAP2 *in vivo*.

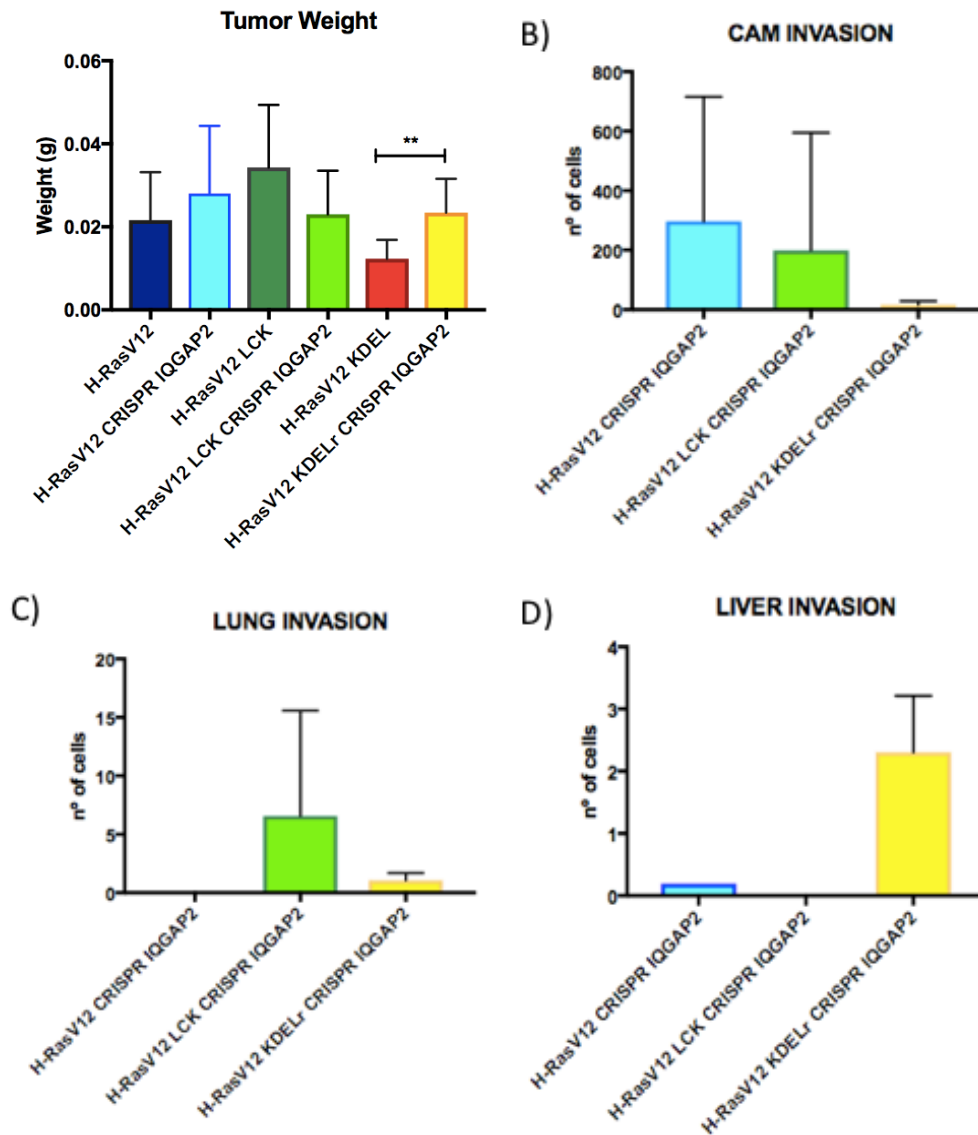


Figure 21 | Study of metastasis in the chick embryo animal model. A) The graphic shows the weight of the tumor formed by IQGAP2 knock out H-RasV12, IQGAP2 knock out H-RasV12 LCK and IQGAP2 knock out H-RasV12 KDELr. **B, C, D)** The graphics show the number of IQGAP2 knock out H-RasV12, IQGAP2 knock out H-RasV12 LCK and IQGAP2 knock out H-RasV12 KDELr that were able to invade the CAM (B), the lungs (C) and the liver (D) when samples were analyzed by quantitative PCR with the specific primers as described in Material and Methods. The bar chart shows the average \pm the SEM and analysis of variance was performed by using the Student t-test. P-value: **, P-value<0.005.

5. DISCUSSION

The concept of space as a key factor in the regulation of Ras functions has been solidly supported by studies demonstrating that Ras proteins are present in different types of membranes (Matallanas *et al.*, 2006). At these distinct sublocalizations, RAS signal is subject to site-specific regulation by scaffold proteins that facilitate the activation of different targets (Casar & Crespo, 2016).

In the present study, we have checked differences between tumor and normal thyroid cells. To do so, we used the already generated PCCL3 H-RasV12, the site-specific ones tethered to LR and GC stable cells lines and their transfected CRISPR/Cas9 IQGAP2 partners. We reduced the levels of IQGAP2 in the LR and GC site-specific Ras signals tumor thyroid cells. Ras signaling arising from GC showed higher migratory and invasive capacity *in vitro*. However, *in vivo*, we were not able to see such changes since we used little number of chick embryos. In this regard, future studies with higher sample size might help providing a better perspective on the role of IQGAP2 *in vivo*, since the results obtained were not significant and incorruptible comparing with the *in vitro* experiments. The *in vitro* data suggest IQGAP2 as a possible thyroid cancer tumor suppressor without decreasing pERK levels suggesting an ERK1/2 independent mode of action.

IQGAPs have been reported to play crucial roles in cancer progression. As IQGAP1 have been described as a tumor promoter, on the contrary, IQGAP2 has been identified as a tumor suppressor in different cancers: such as gastric, liver, prostate and ovarian cancer among others. Some authors have demonstrated that IQGAP2 expression is downregulated in more invasive and metastatic liver cancer cell lines and also in a wide number of human hepatocellular carcinomas (Kumar, Hassan, Pattnaik, Mohapatra & Dixit, 2017). Moreover, other studies have probed IQGAP2 act as tumor suppressor in other hormonal dependent cancer. Besides, Xie *et al.*, (2012) have demonstrated that the reduction of IQGAP2 in prostate cancer might act as a tumor suppressor by significantly decrease E-Cadherin expression by activating AKT pathway. E-cadherin is a cell adhesion protein that is important in the formation of adherent junctions between cells being regulated mostly by the Wnt- β -Catenin signaling pathway. Thyroid cancer has also been related with E-cadherin loss. Ivanova *et al.* (2017) studied the role of E-cadherin and B-catenin in epithelial carcinomas of the thyroid gland. This protein expression was focally retained in membranes and cytoplasm tumor cells of the papillary and follicular thyroid cancers, the less aggressive and metastatic ones whereas in anaplastic thyroid cancers, the more aggressive type, the expression of E-cadherin was almost lost. These suggest that maybe E-cadherin regulation by IQGAP2 could be exerting a crucial role in thyroid tumorigenesis as it does in prostate cancer, another hormone-dependent tumor type.

However, tumor thyroid cells had been untested the role of IQGAP2 so far. We propose that the loss of IQGAP2 scaffold protein might contribute to thyroid cancer pathogenesis probably enhancing metastasis to other organs. As we have seen that is a process that does not involve ERK1/2 we suggest as a possible experiment the determination of E-Cadherin expression levels and of the mediators of the B-catenin-Wnt pathway.

In conclusion, the findings from this study support most of the studies developed before by other groups suggesting that the reduction of the expression of IQGAP2 can promote cancer. In our case IQGAP2 promotes migratory and invasive capacity *in vitro* hypothetically decreasing levels of E-cadherin and β -Catenin.

Therefore, these data could help to the identification of new possible molecular targets to develop drugs against the most aggressive types of thyroid cancer. Due to that, actual therapies that decrease IQGAP2 levels should be taken into account since its reduction seems to decrease tumor weight but not its metastatic potential and even promoting more aggressive phenotype.

6. CONCLUSIONS

- We have probed that the already generated Ha-HRasV12 and HA-KDELr-HRasV12 PCCL3 stable cell lines were correctly transfected with their correspondent construct by immunofluorescence, checking that HA-HRasV12 was distributed throughout all the cell in H-RasV12 PCCL3 cells and HA-HRasV12 colocalized with the GC in H-RasV12 KDELr PCCL3 cells.
- We have been able to generate the IQGAP2 knock out H-RasV12 PCCL3 stable cell lines, seeing a dramatic reduction of IQGAP2 expression by Western blot.
- We have determined that the proliferative behavior was not affected by the absence of IQGAP2, but the migratory and invasive behavior were enhanced when the cells were not express IQGAP2, especially those that Ras signaling arising from GC and it is ERK1/2 independent.
- We have compared the metastatic profile of IQGAP2 knock out H-RasV12, LCK and KDELr PCCL3 stable cell lines, but the unique significative results were observed in the tumor weight between KDELr and IQGAP2 knock out KDELr cells.

7. FUTURE PERSPECTIVES

In the future, PCCL3 H-RasV12 M1 and PCCL3 H-RasV12 CD8 must be transfected to reduce the levels of IQGAP2 and determine the same behaviors that we have looked for. Thus, the role of IQGAP2 scaffold could be compared when H-RasV12 are tethered in all the different site-specific localizations, determining if the loss of IQGAP2 is different depending on the microdomain from which Ras-ERK signaling is arising.

Although the role of IQGAP2 in tumor thyroid cancer cells has not been properly determined yet, these studies could help to raise future perspectives. Given that IQGAP2 scaffold protein modified the migratory and invasive behaviors of tumor thyroid cells in an ERK1/2 independent manner we should check different signaling pathways. As some other authors have correlated the loss of IQGAP2 to a downregulation E-cadherin we think that it could be interesting to analyze its expression levels in all the IQGAP2 knock out PCCL3 H-RasV12 cell lines by Western blot and immunofluorescence.

Moreover, the identification of the proteins that interact with IQGAP2 could help to understand which of these can be mediating the cellular behaviors that we have seen. For it, we suggest as a possible experiment an immunoprecipitation-proteomics assay to check the proteins that bind to IQGAP2. A second one could be the blockage of the interaction of some of the proteins previously identified to check which one is mediating the effects.

8. REFERENCES

- Agudo-Ibáñez, L., Herrero, A., Barbacid, M., & Crespo, P. (2015). H-ras distribution and signaling in plasma membrane microdomains are regulated by acylation and deacylation events. *Molecular and Cellular Biology*, 35(11), 1898–914.
<https://doi.org/10.1128/MCB.01398-14>
- Calvo, F., Agudo-Ibáñez, L., & Crespo, P. (2010). The Ras-ERK pathway: Understanding site-specific signaling provides hope of new anti-tumor therapies. *BioEssays*, 32(5), 412-421.
<https://doi.org/10.1002/bies.200900155>
- Carling, T., & Udelsman, R. (2014). Thyroid Cancer. *Annual Review of Medicine*, 65(1), 125–137. <https://doi.org/10.1146/annurev-med-061512-105739>
- Casar, B., & Crespo, P. (2016). ERK Signals: Scaffolding Scaffolds? *Frontiers in Cell and Developmental Biology*, 4(49), 1–11. <https://doi.org/10.3389/fcell.2016.00049>
- Crespo, P., & Casar, B. (2016). The Chick Embryo Chorioallantoic Membrane as an in vivo Model to Study Metastasis. *Bio-Protocol*, 6(20), e1962.
<https://doi.org/10.21769/BioProtoc.1962>
- Fehrenbacher, N., Bar-Sagi, D., & Philips, M. (2009). Ras/MAPK signaling from endomembranes. *Molecular Oncology*, 3(4), 297–307.
<https://doi.org/10.1016/j.molonc.2009.06.004>
- Fey, D., Matallanas, D., Rauch, J., Rukhlenko, O. S., & Kholodenko, B. N. (2016). The complexities and versatility of the RAS-to-ERK signalling system in normal and cancer cells. *Seminars in Cell and Developmental Biology*, 58, 96-107.
<https://doi.org/10.1016/j.semcdb.2016.06.011>
- Hancock, J. F., & Parton, R. G. (2005). Ras plasma membrane signalling platforms. *Biochemical Journal*, 389(1), 1–11. <https://doi.org/10.1042/BJ20050231>
- Ivanova, K., Ananiev, J., Aleksandrova, E., Ignatova, M.M. & Gulubova, M. (2017). Expression of E- Cadherin/Beta-Catenin in Epithelial Carcinomas of the Thyroid Gland. *Open Access Macedonian Journal of Medical Sciences*, 5(2), 155-159.
<https://doi.org/10.3889/oamjms.2017.043>
- Herrero, A., & Crespo, P. (2016). Tumors topple when ERKs uncouple. *Molecular & Cellular Oncology*, 3(2), e1091875 1-3. <https://doi.org/10.1038/ncomms5839>.Spatial
- Kimura, T., Keymeulen, A. V. A. N., Golstein, J., Fusco, A., Dumont, J. E., & Roger, P. P. (2001). Regulation of Thyroid Cell Proliferation by TSH and Other Factors : A Critical Evaluation of in Vitro Models. *Endocrine Reviews*, 22(5), 631–656.
- Kumar, D., Hassan, M. K., Pattnaik, N., Mohapatra, N., & Dixit, M. (2017). Reduced expression of IQGAP2 and higher expression of IQGAP3 correlates with poor prognosis in cancers. *PLoS ONE*, 12(10), e0186977. <https://doi.org/10.1371/journal.pone.0186977>

- Matallanas, D., Sanz-Moreno, V., Arozarena, I., Calvo, F., Agudo-Ibáñez, L., Santos, E., Berciano, M. T. & Crespo, P. (2006). Distinct utilization of effectors and biological outcomes resulting from site-specific Ras activation: Ras functions in lipid rafts and Golgi complex are dispensable for proliferation and transformation. *Molecular and Cellular Biology*, 26(1), 100–116. <https://doi.org/10.1128/MCB.26.1.100-116.2006>
- Mccubrey, J. A., Steelman, L. S., Chappell, W. H., Abrams, S. L., Montalto, G., Cervello, M., Nicoletti, F., Fagone, P., Malaponte, G., Mazzarino, M. C., Candido, S., Libra, M., Bäsecke, J., Mijatovic, S., Maksimovic-Ivanic, D., Milella, M., Tafuri, A., Cocco, L., Evangelisti, C., Chiarini, F. & Martelli, A. M. (2012). Mutations and Dereglulation of Ras/Raf/MEK/ERK and PI3K/ PTEN/Akt/mTOR Cascades Which Alter Therapy Response. *Oncotarget*, 33(9), 954–987. Retrieved from www.impactjournals.com/oncotarget
- Naoum, G. E., Morkos, M., Kim, B., & Arafat, W. (2018). Novel targeted therapies and immunotherapy for advanced thyroid cancers. *Molecular Cancer*, 17(1), 1-15. <https://doi.org/10.1186/s12943-018-0786-0>
- Neuzillet, C., Tijeras-Raballand, A., De Mestier, L., Cros, J., Faivre, S., & Raymond, E. (2014). MEK in cancer and cancer therapy. *Pharmacology and Therapeutics*, 141(2), 160–171. <https://doi.org/10.1016/j.pharmthera.2013.10.001>
- Nikiforov, Y. E., & Nikiforova, M. N. (2011). Molecular genetics and diagnosis of thyroid cancer. *Nature Reviews Endocrinology*, 7(10), 569-580. <https://doi.org/10.1038/nrendo.2011.142>
- O. Shaul, M. V. M. and D. I. (1996). *Cell Cycle Control. Annals of Botany* (Vol. 78). https://doi.org/10.1007/978-1-4939-0888-2_6
- Riesco-Eizaguirre, G., & Santisteban, P. (2007). New insights in thyroid follicular cell biology and its impact in thyroid cancer therapy. *Endocrine-Related Cancer*, 14(4), 957–977. <https://doi.org/10.1677/ERC-07-0085>
- Roberts, P. J., & Der, C. J. (2007). Targeting the Raf-MEK-ERK mitogen-activated protein kinase cascade for the treatment of cancer. *Oncogene*, 26(22), 3291–3310. <https://doi.org/10.1038/sj.onc.1210422>
- Smith, J. M., Hedman, A. C., & Sacks, D. B. (2015). IQGAPs choreograph cellular signaling from the membrane to the nucleus. *Trends in Cell Biology*, 25(3), 171-184. <https://doi.org/10.1016/j.tcb.2014.12.005>
- White, C. D., Brown, M. D., & Sacks, D. B. (2009). IQGAPs in cancer: A family of scaffold proteins underlying tumorigenesis. *FEBS Letters*, 583(12), 1817-1817. <https://doi.org/10.1016/j.febslet.2009.05.007>
- White, C. D., Khurana, H., Gnatenko, D. V, Li, Z., Odze, R. D., Sacks, D. B., & Schmidt, V. A. (2010). IQGAP1 and IQGAP2 are Reciprocally Altered in Hepatocellular Carcinoma.

- BMC Gastroenterology*, 10, 125. <https://doi.org/10.1186/1471-230X-10-125>
- Zaballos, M. A., & Santisteban, P. (2017). Signaling in thyroid cancer Key signaling pathways in thyroid cancer. <https://doi.org/10.1530/JOE-17-0266>
- Xie, Y., Yan, J., Cutz, J. C., Rybak, A. P., He, L., Wei, F., Kapoor, A., Schmidt, V.A., Tao, L. & Tang, D. (2012). IQGAP2, A candidate tumour suppressor of prostate tumorigenesis. *Biochimica et Biophysica Acta - Molecular Basis of Disease*, 1822(6), 875–884. <https://doi.org/10.1016/j.bbadis.2012.02.019>